Astron. Astrophys. 344, 848–856 (1999)

ASTRONOMY AND ASTROPHYSICS

Very young massive stars in the Small Magellanic Cloud, revealed by *HST*⋆

M. Heydari-Malayeri[1], **M.R. Rosa**[2,⋆⋆], **H. Zinnecker**[3], **L. Deharveng**[4], **and V. Charmandaris**[1]

[1] DEMIRM, Observatoire de Paris, 61 Avenue de l'Observatoire, F-75014 Paris, France
[2] Space Telescope European Coordinating Facility, European Southern Observatory, Karl-Schwarzschild-Strasse 2, D-85748 Garching bei München, Germany
[3] Astrophysikalisches Institut Potsdam, An der Sternwarte 16, D-14482 Potsdam, Germany
[4] Observatoire de Marseille, 2 Place Le Verrier, F-13248 Marseille Cedex 4, France

Received 1 December 1998 / Accepted 18 January 1999

Abstract. High spatial resolution imaging with the *Hubble Space Telescope* allowed us to resolve the compact H II region N 81 lying in the Small Magellanic Cloud (SMC). We show the presence of a tight cluster of newborn massive stars embedded in this nebular "blob" of $\sim 10''$across. This is the first time the stellar content and internal morphology of such an object is uncovered. These are among the youngest massive stars in this galaxy accessible to direct observations at ultraviolet and optical wavelengths. Six of them are grouped in the core region of $\sim 2''$diameter, with a pair of the main exciting stars in the very center separated by only $0''.27$ or 0.08 pc. The images display violent phenomena such as stellar winds, shocks, ionization fronts, typical of turbulent starburst regions. Since the SMC is the most metal-poor galaxy observable with very high angular resolution, these observations provide important templates for studying star formation in the very distant metal-poor galaxies which populate the early Universe.

Key words: stars: early-type – stars: Wolf-Rayet – ISM: dust, extinction – ISM: H II regions – ISM: individual objects: N 81 (SMC) – galaxies: Magellanic Clouds

1. Introduction

It is now generally believed that massive stars form in dense cores of molecular clouds. Initially, they are enshrouded in dusty remains of the molecular material, and, therefore, are not observable in ultraviolet and visible light. At this stage they can only be detected indirectly at infrared and radio wavelengths, emitted respectively by the surrounding dust and by the ionized stellar winds. At a later stage the far-UV photons dissociate the molecules and ionize the atoms creating ultracompact H II regions. Eventually, the natal molecular cloud is ionized to become a compact H II region. As the ionized volume of gas increases, the advancing ionization front of the H II region reaches the cloud border. The ionized gas then flows away into the interstellar medium according to the so-called champagne effect (Tenorio-Tagle 1979, Bodenheimer et al. 1979). From this time on the opacity drops and the newborn stars become accessible to observation in the ultraviolet and visible.

The youngest H II regions that can be penetrated with ultraviolet and optical instruments provide therefore the best opportunities for a *direct* access to massive stars at very early stages of their evolution. Because of the small timescales involved, it is difficult to catch the most massive stars just at this very point in their evolution, namely when the young H II regions emerge from the associated molecular clouds. Contrary to the situation in the Galaxy, where interstellar extinction in the line of sight is generally high, the Magellanic Clouds, especially the SMC, provide an environment where the sites of massive star formation are accessible without additional foreground extinction.

Our search for such very young, emerging H II regions in the Magellanic Clouds started almost a decade ago on the basis of ground-based observations at the European Southern Observatory. The result was the discovery of a distinct and very rare class of H II regions in the Magellanic Clouds, that we called high-excitation compact H II "blobs" (HEBs). The reason for this terminology was that no features could be distinguished with those telescopes. So far only five HEBs have been found in the LMC: N159-5, N160A1, N160A2, N83B-1, and N11A (Heydari-Malayeri & Testor 1982, 1983, 1985, 1986, Heydari-Malayeri et al. 1990) and two in the SMC: N88A and N 81 (Testor & Pakull 1985, Heydari-Malayeri et al. 1988a).

In contrast to the typical H II regions of the Magellanic Clouds, which are extended structures (sizes of several arc minutes corresponding to more than 50 pc, powered by a large number of exciting stars), HEBs are very dense and small regions ($\sim 5''$to $10''$in diameter corresponding to ~ 1.5–3.0 pc). HEBs are, in general, heavily affected by local dust (Heydari-Malayeri et al. 1988a, Israel & Koornneef 1991). They are probably the

Send offprint requests to: M. Heydari-Malayeri (heydari@obspm.fr)

⋆ Based on observations with the NASA/ESA Hubble Space Telescope obtained at the Space Telescope Science Institute, which is operated by the Association of Universities for Research in Astronomy, Inc., under NASA contract NAS 5-26555.

⋆⋆ Affiliated to the Astrophysics Division, Space Science Department of the European Space Agency.

final stages in the evolution of the ultracompact H II regions whose Galactic counterparts are detected only at infrared and radio frequencies (Churchwell 1990). Because of the contamination by strong nebular background no direct information about the exciting stars of HEBs has been achievable with ground-based telescopes. Furthermore, it is not known whether a single hot object or several less massive stars are at work there.

The compact H II "blob" N 81 (Henize 1956, other designations: DEM138 in Davies et al. 1976, IC 1644, HD 7113, etc.) lies in the Shapley Wing at $\sim 1\overset{\circ}{.}2$ (~ 1.2 kpc) from the main body of the SMC. Other H II regions lying towards the Wing are from west to east N83, N84, N88, N89, and N90. A study of N 81 carried out a decade ago (Heydari-Malayeri et al. 1988a), revealed some of its physical characteristics: age of 1 to 2.5 million years, mass of ionized gas amounting to $\sim 350\,M_{\odot}$, low metal content typical of the chemical composition of the SMC, gas density of ~ 500 cm^{-3}, electron temperature of 14 100° K, etc. However, the study suffered from a lack of sufficient spatial resolution and could not be pursued by available Earth-bound facilities. More specifically, the exciting star(s) remained hidden inside the ionized gas. It was not possible to constrain the theoretical models as to the nature of the exciting source(s) and choose among various alternatives (Heydari-Malayeri et al. 1988a). This is, however, a critical question for theories of star formation.

The use of *HST* is therefore essential for advancing our knowledge of these objects. Here we present the results of our project GO 6535 dedicated to direct imaging and photometry of the "blobs" as a first step in their high-resolution study. A "true-color" high-resolution image and a brief account of the results for the layman were presented in a NASA/HST/ESA Press Release 98-25, July 23, 1998 (Heydari-Malayeri et al. 1998: http://oposite.stsci.edu/pubinfo/pr/1998/25).

2. Observations and data reduction

The observations of N 81 described in this paper were obtained with the Wide Field Planetary Camera 2 (WFPC2) on board the *HST* on September 4, 1997. The small size of N 81 makes it an ideal target for the $36''$-field of WFPC2. We used several wide- and narrow-band filters (F300W, F467M, F410M, F547M, F469N, F487N, F502N, F656N, F814W) with two sets of exposure times (short and long). In each set we repeated the exposures twice with ~ 5 pixel offset shifts in both horizontal and vertical direction. This so-called dithering technique allowed us to subsequently enhance the sampling of the point spread function (PSF) and improve our spatial resolution by $\sim 20\%$. The short exposures, aimed at avoiding saturation of the CCD by the brightest sources, range from 0.6 sec (F547M) to 20 sec (F656N). The long exposures range from 8 sec (F547M) to 300 sec (F656N & F469N).

The data were processed through the standard *HST* pipeline calibration. Multiple dithered images where co-added using the STSDAS task *drizzle* (Fruchter & Hook 1998), while cosmic rays were detected and removed with the STSDAS task *crrej*. Normalized images were then created using the total exposure times for each filter. To extract the positions of the stars, the routine *daofind* was applied to the images by setting the determination threshold to 5σ above the local background level. The photometry was performed setting a circular aperture of 3–4 pixels in radius in the *daophot* package in STSDAS.

A crucial point in our data reduction was the sky subtraction. For most isolated stars the sky level was estimated and subtracted automatically using an annulus of 6–8 pixel width around each star. However this could not be done for several stars located in the central region of N 81 due to their proximity. In those cases we carefully examined the PSF size of each individual star (FWHM ~ 2 pixels, corresponding to $0''\!.09$ on the sky) and did an appropriate sky subtraction using the mean of several nearby off-star positions. To convert into a magnitude scale we used zero points in the Vegamag system, that is the system where Vega is set to zero mag in Cousin broad-band filters. The magnitudes measured were corrected for geometrical distortion, finite aperture size (Holtzman et al. 1995), and charge transfer efficiency as recommended by the HST Data Handbook. The photometric errors estimated by *daophot* are smaller than 0.01 mag for the brighter (14–15 mag) stars, while they increase to ~ 0.2 mag for 19 mag stars.

We note that the filter F547M is wider than the standard Strömgren y filter. To evaluate the presence of any systematic effects in our photometry and color magnitude diagrams due to this difference in the filters, we used the STSDAS package *synphot*. Using synthetic spectra of hot stars, with spectral types similar to those found in H II regions, we estimated the difference due to the *HST* band-passes to be less than 0.002 mag, which is well within the photometric errors.

The "true-color" image of N 81 (Heydari-Malayeri et al. 1998) was assembled from three separate WFPC2 images using the IRAF external package COLOR task *rgbsum*. The basic images were the ultraviolet (F300W) and the hydrogen emission blue and red lines Hβ (F487N) and Hα (F656N).

Two line intensity ratio maps were secured using the normalized Hα, Hβ and [O III] λ5007 (F502N) images (Sect. 3.2 and Sect. 3.3). In order to enhance the S/N ratio in the fainter parts, each image was first smoothed using a 2×2-pixel Gaussian filter.

3. Results

3.1. Overall view

The WFPC2 imaging, in particular the I band filter, reveals some 50 previously unknown stars lying towards N 81, where not even one was previously observable. Six of them are grouped in the core region of $\sim 2''$ wide, as displayed in Fig. 1. The brightest ones are identified by numbers in Fig. 2. See also the true-color version of this image accompanying the *HST* Press Release (Heydari-Malayeri et al. 1998). Two bright stars (#1 & #2) occupy a central position and are probably the main exciting sources of the H II region. Only $0''\!.27$ apart on the sky (projected separation ~ 0.08 pc), they are resolved in the WFPC2 images (Fig. 3).

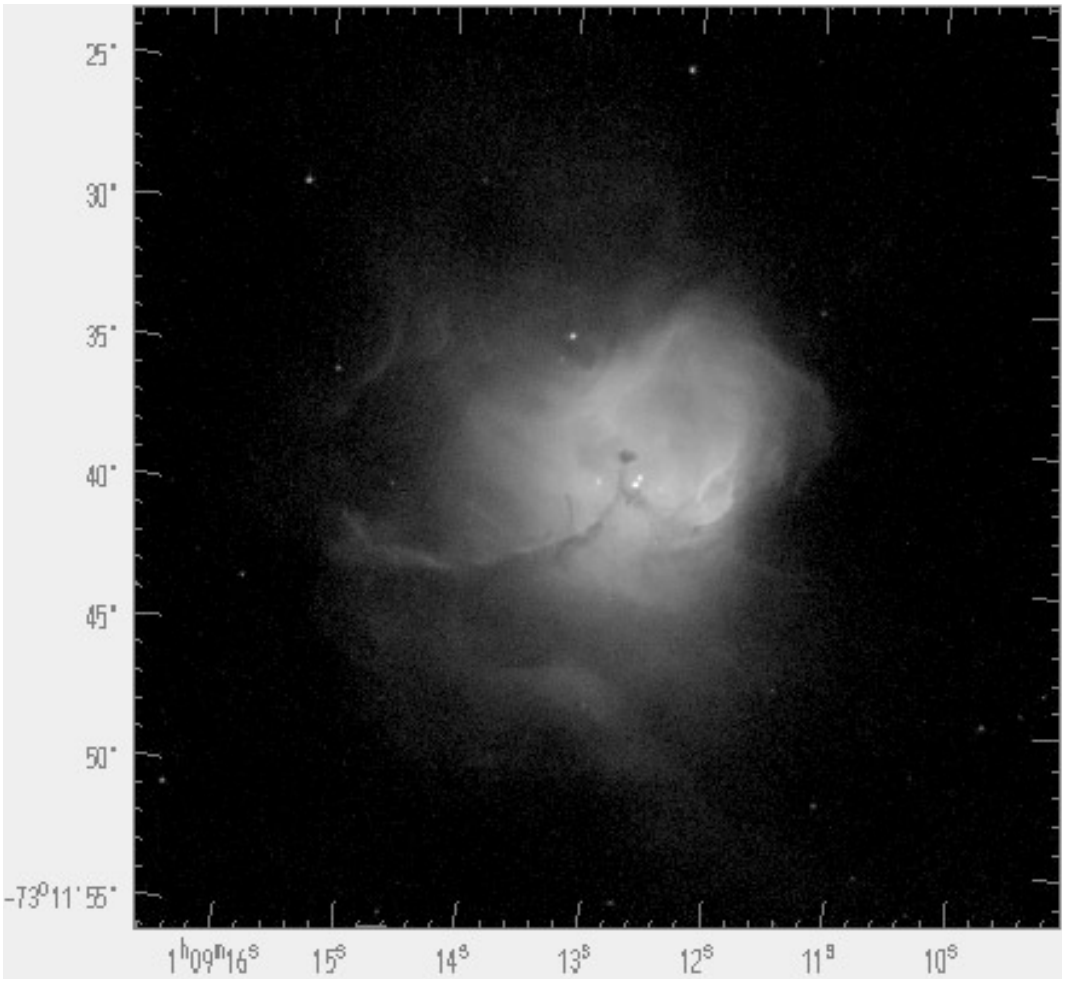

Fig. 1. The Small Magellanic Cloud compact nebula N 81 in Hα emission. The two bright stars (#1 & #2, see Fig. 2) lying below the small central absorption "hole" are the main exciting stars. See Fig. 3 for a close-up of the inner regions. The field size is $\sim 33'' \times 33''$($\sim 10 \times 10$ pc). North is up and east is left.

Two prominent dark lanes divide the nebula into three lobes. One of the lanes ends in a magnificent curved plume more than 15″(4.5 pc) in length. The absorption features are probably parts of the molecular cloud associated with the H II region (Sect. 4.2). The extinction due to dust grains in those directions amounts to ~ 1 mag as indicated by the Hα/Hβ map (Sect. 3.2). A conspicuous absorption "hole" or dark globule of radius $\sim 0''.25$ is situated towards the center of the H II region, where the extinction reaches even higher values. The apparent compact morphology of this globule in the presence of a rather violent environment is intriguing. We explore some possibilities of its origin in Sect. 4.1.

An outstanding aspect is the presence of arched filaments, gaseous wisps, and narrow ridges produced by powerful stellar winds and shocks from the hot, massive stars. We are therefore witnessing a very turbulent environment typical of young regions of star formation. The two bright ridges lying west of stars #1 & #2 are probably ionization/shock fronts. The filamentary and wind induced structures are best seen in Fig. 4, which presents an unsharp masking image of N 81 in Hα without large scale structures. In order to remove these brightness variations and enhance the high spatial frequencies, a digital "mask" was created from the Hα image. First the Hα image was convolved by a 2×2-pixel Gaussian, and then the smoothed frame was subtracted from the original Hα image. Interestingly, the inspection of the orientation of these arched filaments suggests the presence of at least three sources of stellar winds: stars #1 & #2 jointly, #3, and probably #11, which are the four brightest blue stars of the cluster.

3.2. Extinction

A map of the Hα/Hβ Balmer decrement is presented in Fig. 5a. The ratio reaches its highest values towards the dark lanes (~ 3.8), the western ridges (~ 4.5), and the dark globule (~ 4.5). This latter value is very close to the highest ratio (4.3) expected for a medium in which dust is locally mixed with gas. The dark "hole", while present, does not show up prominently in Fig. 5a, because it is small ($\sim 0''.25$ across corresponding to $\sim 15\,000$ AU) and the binning by convolution used to enhance

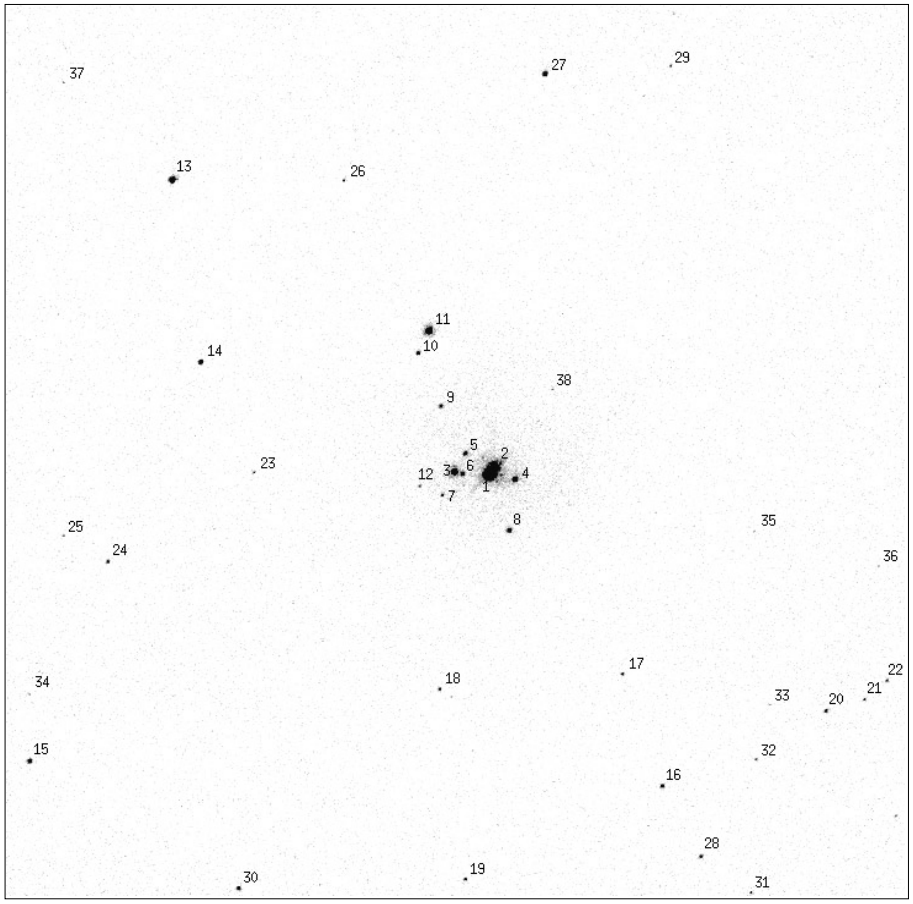

Fig. 2. A WFPC2 image taken using the Strömgren y filter where only the brighter stars are labelled. The photometry of the brightest subsample is presented in Table 1. The field size and orientation are the same as in Fig. 1.

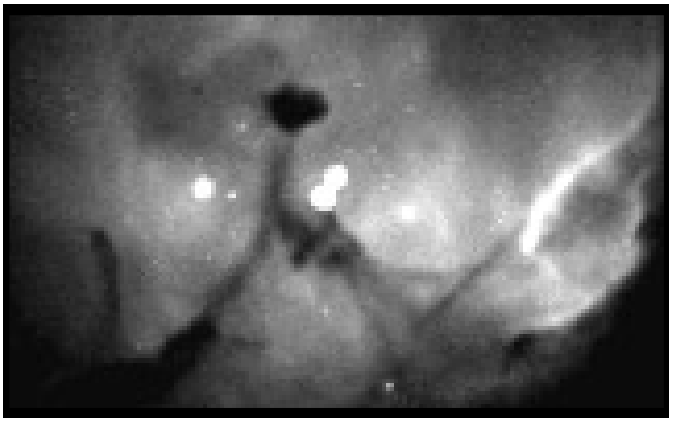

Fig. 3. A close-up of the inner part of N 81 in Hα emission. The two brighter stars (#1 & #2), 0$''$.27 apart, and the absorption features as well as the western ridges, representing ionization/shock fronts, stand out prominently. The inner ridge lies at a projected distance of ~ 0.7 pc from the two main stars; the outer one at ~ 1.0 pc. Field size $\sim 7''.4 \times 4''.6$. ($\sim 2.2 \times 1.4$ pc).

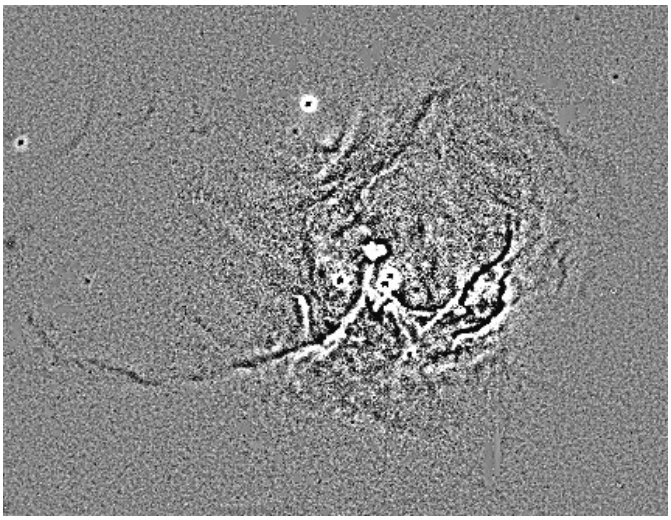

Fig. 4. An unsharp masking image of N 81 obtained in Hα, which highlights the filamentary patterns of the nebula (see the text). Field size $\sim 20'' \times 16''$(6.0 $\times$ 4.7 pc), orientation as in Fig. 1.

the S/N ratio in the fainter parts (Sect. 2) has reduced the line ratio. The high Hα/Hβ ratios and the fact that the interstellar extinction is known to be small towards the SMC (Prévot et al. 1984) support the idea that dust is local and probably mixed with gas in this young H II region. Furthermore, the high resolution observations show that the extinction towards N 81 is generally higher than previously believed. A mean Hα/Hβ= 3.30 corresponds to A_V = 0.40 mag (c(Hβ) = 0.20), if the interstellar reddening law is used. For comparison, the ground-based observations had yielded Hα/Hβ values of 3.05 (Heydari-Malayeri

Table 1. Photometry of the brightest stars towards N 81

Star number	α (J2000)	δ (J2000)	v (F410M)	b (F467M)	y (F547M)	He II (F469N)	wide U (F300W)	I (F814W)
1	01:09:13.05	–73:11:38.27	14.04	14.28	14.38	14.30	12.64	15.80
2	01:09:13.03	–73:11:38.03	14.50	14.76	14.87	14.81	12.88	14.90
3	01:09:13.35	–73:11:38.37	15.83	16.02	16.10	16.02	14.37	16.10
4	01:09:12.83	–73:11:38.31	17.20	17.48	17.41	17.46	15.65	17.17
5	01:09:13.28	–73:11:37.63	18.09	18.24	18.29	18.23	16.85	18.37
6	01:09:13.28	–73:11:38.39	18.12	18.19	18.11	18.13	17.30	17.59
7	01:09:13.43	–73:11:39.29	19.25	19.69	19.64	19.27	18.15	19.06
8	01:09:12.82	–73:11:40.23	18.00	17.99	17.84	17.90	16.68	17.57
9	01:09:13.54	–73:11:36.01	18.66	18.87	18.80	18.83	17.60	18.69
10	01:09:13.80	–73:11:34.17	18.13	18.46	18.47	18.38	17.01	18.49
11	01:09:13.74	–73:11:33.31	15.38	15.64	15.74	15.64	13.85	16.11
13	01:09:16.08	–73:11:29.07	16.42	16.57	16.65	16.52	15.36	16.67
14	01:09:15.61	–73:11:35.63	17.76	17.90	17.99	17.86	16.50	18.14
15	01:09:16.58	–73:11:51.21	18.73	18.49	18.10	18.21	19.22	17.21
16	01:09:11.22	–73:11:48.87	18.37	18.59	18.60	18.58	17.32	18.57
17	01:09:11.69	–73:11:45.00	19.18	19.13	19.39	19.23	18.05	19.07
18	01:09:13.22	–73:11:46.43	19.07	19.26	19.39	19.16	18.00	19.13
24	01:09:16.16	–73:11:43.49	20.44	19.67	19.10	20.58	–	18.10
27	01:09:13.07	–73:11:23.24	18.81	18.38	17.74	18.13	–	16.82

et al. 1988a) and 2.97 (Caplan et al. 1996, using a circular diaphragm of 4.″89 in diameter). We remark that the Balmer ratio decreases with decreasing spatial resolution. This provides another indication that dust is concentrated towards the inner parts of N 81.

3.3. Nebular emission

The [O III]λ5007/Hβ intensity map (Fig. 5b) reveals a relatively extended high-excitation zone with a mean value of $\sim$4.8. The highest intensity ratio, $\sim$5.5, belongs to the region of shock/ionization fronts represented by the two bright western ridges (Fig. 3). It is not excluded that collisional excitation of the O^{++} ions by shocks contributes to the high value of the ratio in that region. Another high excitation zone runs from the east of star #9 to the south. The remarkable extension of the [O III]λ5007/Hβ ratio suggests that the O^{++} ions in N 81 occupy almost the same zone as H^+. This is in agreement with our previous chemical abundance determination results (Heydari-Malayeri et al. 1988a) showing that more than 80% of the total number of oxygen atoms in N 81 are in the form of O^{++}. The extension of the ratio also suggests that the H II region is not powered by one central, but by several separate hot stars.

We measure a total Hβ flux F(Hβ) = 7.69 $\times$ 10^{-12} erg cm^{-2} s^{-1} above 3σ level for N 81 without the stellar contribution and accurate to $\sim$3%. Correcting for a reddening coefficient of c(Hβ) = 0.20 (Sect. 3.2) gives F_0(Hβ) = 1.20 $\times$ 10^{-11} erg cm^{-2} s^{-1}. From this a Lyman continuum flux of N_L = 1.36 $\times$ 10^{49} photons s^{-1} can be worked out if the H II region is assumed to be ionization-bounded. A single main sequence star of type O6.5 or O7 can account for this ionizing UV flux (Vacca et al. 1996, Schaerer & de Koter 1997). However, this is apparently an underestimate since the dust grains mixed with gas would considerably absorb the UV photons, and moreover the H II region is probably density-bounded, since one side of it has been torn open towards the interstellar medium.

3.4. Stellar content

The results of the photometry for the brightest stars are presented in Table 1, where the star number refers to Fig. 2. The color-magnitude diagram y versus $b-y$ is displayed in Fig. 6a. It shows a blue cluster centered on Strömgren colors $b - y = -0.05$, or $v - b = -0.20$, typical of massive OB stars (Relyea & Kurucz 1978, Conti et al. 1986). This is confirmed by the $U-I$ colors deduced from Table 1. Almost all these stars lie within the H II region and we are in fact viewing a starburst in this part of the SMC. We may neglect some of the ionizing stars if they lie deeper in the molecular cloud and are affected by larger extinctions. The three red stars (#15, #24, and #27), located outside the H II region, show up particularly in the true-color image (Heydari-Malayeri et al. 1998) and are probably evolved stars not belonging to the cluster. The two main exciting stars (#1 and #2) stand out prominently on the top of the color-magnitude diagram.

One can estimate the luminosity of the brightest star of the cluster (#1), although in the absence of spectroscopic data this is not straightforward. Using a mean reddening of A_V = 0.4 mag (Sect. 3.2), and a distance modulus $M-m$ = 19.0 (corresponding to a distance of 63.2 kpc, e.g. Di Benedetto 1997 and references therein), we find a visual absolute magnitude M_V = –5.02 for star #1. If a main sequence star, this corresponds to an O6.5V according to the calibration of Vacca et al. (1996) for Galactic stars. The corresponding luminosity and mass would

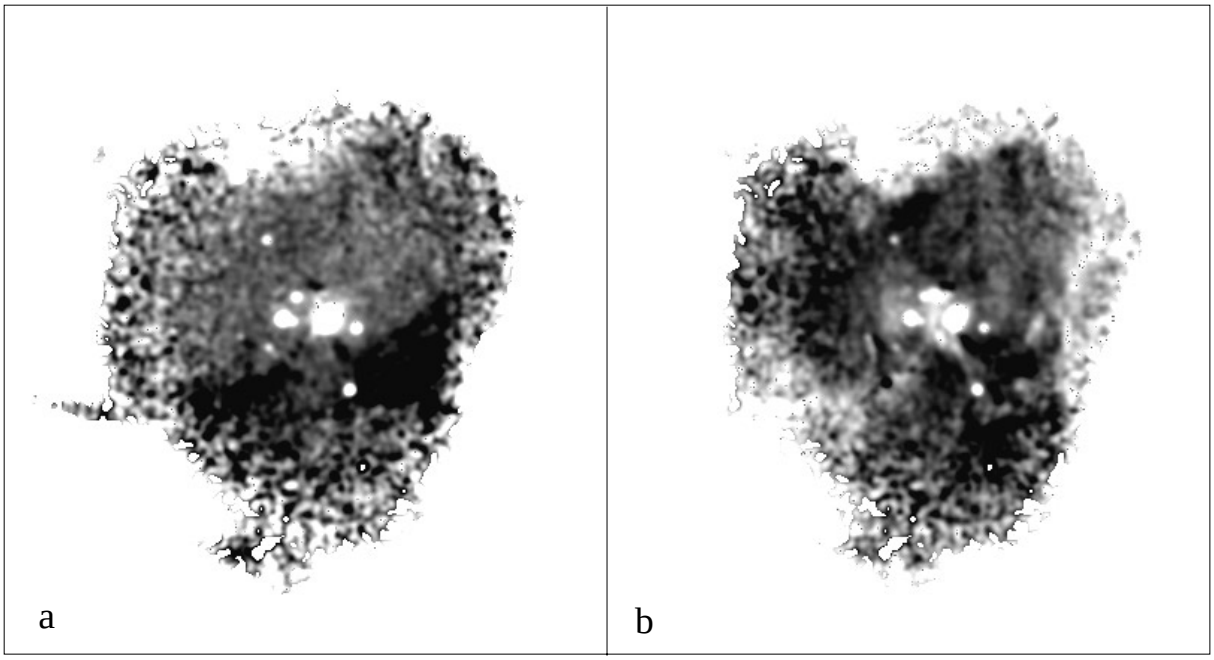

Fig. 5a and b. Line intensity ratios in the central part of N 81. The darker the color the higher the ratio. White spots are stars; see Fig. 2 for their identification. **a** Balmer decrement Hα/Hβ. Its mean value over the region is 3.30 and the ratio goes up to $\sim$ 4.5 towards the central small absorption "hole". The spur extending to the left is the bright end of the eastern absorption lane. **b** The [O III]λ5007/Hβ ratio. It is everywhere higher than 4.5 and rises to more than 6.

be *log L* = 5.49 $L_{\odot}$ and M = 41 $M_{\odot}$. The star may be more massive than this, since sub-luminosity and/or peculiar extinction would be consistent with extreme youth (Walborn et al. 1999).

The images obtained through a narrow-band filter (F469N) centered on the He II 4686 Å line were compared with those using the broad-band filter representing the Strömgren b (F467M). The resulting photometry is displayed in the color-magnitude diagram shown in Fig. 6b. Interestingly, three stars show an apparent He II excess. However, one should note that since two of these (#27 and #15) are red types (Fig. 2, and the true-color image in Heydari-Malayeri et al. 1998), such a narrow-band enhancement could also be due to an artifact of molecular absorption bands throughout the spectra. On the other hand, the third star (#7) is blue and has stronger apparent He II emission. This star lies deep in the core of the star cluster/H II region where the nebular excitation is high. It may be a Wolf-Rayet or Ofpe/WN candidate in the SMC.

4. Discussion and concluding remarks

4.1. Morphology of N 81

N 81 is a young H II region whose moving ionization front has reached the surface of its associated molecular cloud (see Sect. 4.2), as predicted by the champagne model (Tenorio-Tagle 1979, Bodenheimer et al. 1979). Ionized gas is pouring out into the interstellar medium with a relative velocity of 4 km s^{-1} (Sect. 4.2). The bright central core of N 81 is presumably a cavity created by the stellar photons on the surface of the molecular cloud. The two bright ridges lying at projected distances of $\sim$ 0.7 and $\sim$ 1.0 pc west of stars #1 & #2 (Fig. 3) are probably parts of the cavity seen edge-on. They represent ionization/shock fronts advancing in the molecular cloud. The higher excitation zones, indicated by the [O III]/Hβ map (Sect. 3.3), may be parts of the cavity surface situated perpendicularly to the line of sight. The H II region is probably ionization-bounded in those directions. The outer, diffuse areas with fainter brightness (Fig. 1) are the champagne flow in which strong winds of massive stars have given rise to the filamentary pattern.

The absorption lanes and the the dark globule may represent the denser, optically thick remains of the natal molecular cloud which have so far survived the action of harsh ultraviolet photons of the exciting stars. High resolution imaging observations by *HST* have shown the presence of massive dust pillars inside the Galactic H II region M16 (Hester et al. 1996) and more recently in the LMC giant H II region 30 Dor (Scowen et al. 1998, Walborn et al. 1999). By comparison, the dark globule in N 81 may be the summit of such a dust pillar in which second generation stars may be forming. To further investigate this idea, a follow-up high-resolution near-IR imaging of the central region is essential. At longer wavelengths we are less affected by the absorption and we will be able to probe deeper into the core of the globule.

4.2. Molecular cloud

The molecular cloud associated with N 81 has been observed during the ESO-SEST survey of the CO emission in the Magellanic Clouds. Israel et al. (1993) detected ^{12}CO (1-0) emission

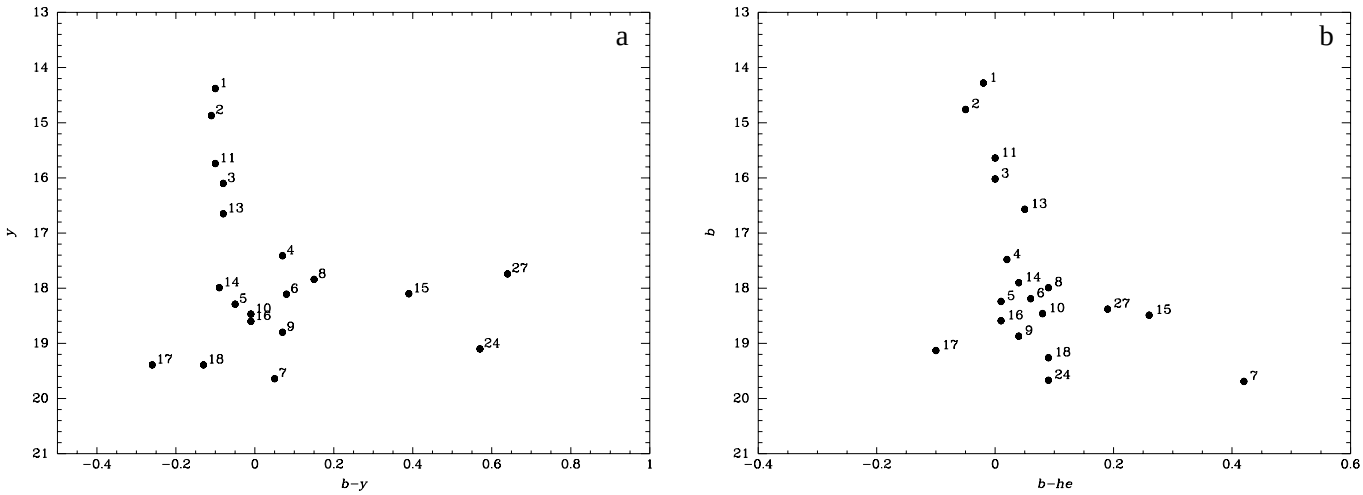

Fig. 6a and b. Color-magnitude diagrams of the brightest stars revealed towards the SMC compact H II region N 81. **a** y versus $b-y$, based on WFPC2 imaging with the Strömgren filters b (F467M) and y (F547). **b** b versus $b-$He II showing the He II 4686 excess, based on narrow-band filter F469N and broad-band continuum F467M.

at two points towards N 81 using a resolution of 43″(∼ 13 pc, or ∼ 4 times the size of the H II region). The brighter component has a main beam brightness temperature of 375 mK, a line width of 2.6 km s^{-1} and a LSR velocity of 152 km s^{-1}. The molecular emission velocity is in agreement with the velocity of the ionized gas V_{LSR} = 147.8 km s^{-1} which we measured on the basis of high dispersion Hβ spectroscopy (Heydari-Malayeri et al. 1988a). The difference of 4.2 km s^{-1} is probably due to the local motion of the ionized gas streaming into the interstellar medium towards the observer. The molecular cloud is brighter than those detected towards the neighboring H II regions N76, N78, and N80, but is weaker than that associated with N84 which has a distinct velocity (168 km s^{-1}). We do not know the size, the morphology, nor the mass of the molecular cloud, and we cannot localize the H II region N 81 with respect to it.

The SMC is known to have an overall complex structure with several overlapping neutral hydrogen layers (McGee & Newton 1981). We used the recent observations by Stanimirovic et al. (1998) to examine the H I emission towards N 81. The authors combine new Parkes telescope observations with an ATCA (Australia Telescope Compact Array) aperture synthesis mosaic to obtain a set of images sensitive to all angular (spatial) scales between 98″(30 pc) and 4°(4 kpc) in order to study the large-scale H I structure of the SMC. An H I concentration focused on N84/N83 extends eastward until N 81 (∼ 30′apart). The H I spectra towards N 81 and N83/N84 show complex profiles ranging from ∼ 100 to 200 km s^{-1} with two main peaks at ∼ 120 and 150 km s^{-1} but spread over tens of km s^{-1}. The corresponding column densities are 3.94×10^{21} and 5.29×10^{21} atoms cm^{-2} respectively. In consequence, the correlation between the H I and CO clouds towards N 81 does not seem simple.

The WFPC2 images reveal a turbulent nebula in which arc-shaped features are sculpted in the ionized gas under the action of violent shocks, ionization fronts, and stellar winds. The presence of shocks in N 81 was evoked by Israel & Koornneef (1988) in order to explain the infrared molecular hydrogen emission which they detected towards this object. H_2 emission may be caused either by shock excitation due to stars embedded in a molecular cloud or by fluorescence of molecular material in the ultraviolet radiation field of the OB stars exciting the H II region. According to these authors, shock excitation of H_2 is only expected very close to (within 0.15 pc of) the stars, while radiative excitation can occur at larger distances (∼ 1 to 2 pc). Our *HST* observations suggest that the radiative mechanism is the dominant one, since the shock/ionization fronts are situated at projected distances larger than 0.15 pc from the exciting stars (Sect. 4.1).

4.3. Star formation

These observations are a breakthrough in the investigation of the exciting source of N 81. This compact H II region is not powered by a single star, but by a small group of newborn massive stars. This result is important not only for studying the energy balance of the H II region, but also because it presents new evidence in support of collective formation of massive stars. Recent findings suggest that massive star formation is probably a collective process (see, e.g., Larson 1992 and references therein, Bonnell et al. 1998). This is also in line with the results of high-resolution, both ground-based and space observations (Weigelt & Baier 1985, Heydari-Malayeri et al. 1988b, Walborn et al. 1995a), in particular the resolution of the so-called Magellanic supermassive stars into tight clusters of very massive components (Heydari-Malayeri & Beuzit 1994 and references therein). It should however be emphasized that these cases pertain to relatively evolved stellar clusters. They are not associated with compact H II regions, probably because the hot stars have had enough time to disrupt the gas.

N 81 is a rare case in the SMC since a small cluster of massive stars is caught almost at birth. It provides a very good chance to check the history of massive star evolution (de Koter

et al. 1997). Massive stars are believed to enter the main sequence while still veiled in their natal molecular clouds (Yorke & Krügel 1977, Shu et al. 1987, Palla & Stahler 1990, Beech & Mitalas 1994, Bernasconi & Maeder 1996) implying that these stars may already experience significant mass loss through a stellar wind, while still accreting mass from the parental cloud. This point constitutes an important drawback for current models of massive star evolution since, contrary to the assumption of the earlier models, a proper zero-age-main-sequence mass may not exist for these stars (Bernasconi & Maeder 1996). As shown by Fig. 4, the most massive stars of the cluster, i.e. stars #1, #2, #11, and #3, seem to be at the origin of stellar winds carving the surrounding interstellar medium. Also, if still younger massive stars are hidden inside the cental dark globule, they can participate in the emission of strong winds.

Another interesting aspect is the small size of the starburst that occurred in N 81. Apparently, only a dozen massive stars have formed during the burst, in contrast to the neighboring region N83/N84 which is larger and richer (Hill et al. 1994). The contrast to the SMC giant region N66 (NGC346), which has produced a plethora of O stars (Massey et al. 1989), is even more striking. The difference may not be only due to the sizes of the original molecular clouds but also to their environments. N 81 is an isolated object far away from the more active, brighter concentrations of matter. Star formation may be a local event there, while for N66 and its neighboring regions, N76, N78, and N80, external factors may have played an active role in triggering the starburst. Judging from their radial velocities (Israel et al. 1993), the molecular clouds associated with the H II regions of the Wing seem to be independent from each other, and star formation has not probably propagated from one side to the other. On the other hand, according to Hunter (1995), massive stars formed in very small star-forming regions appear to have a very different mass function, implying that different sizes of star-forming events can have different massive star products. However, the resolution of this question needs more observational data.

We may have overlooked a distinct co-spatial population of lower mass stars towards N 81, as our short exposure WFPC2 images were aimed at uncovering the brightest massive stars lying inside the ionized H II region. Note that the Orion Nebula, which contains a low-mass population (Herbig & Terndrup 1986, McCaughrean & Stauffer 1994, Hillenbrand 1997), would have the same size as N 81 if placed in the SMC. Interestingly, the I band image shows many red stars not visible in the blue bands, a few fainter ones lying close to stars #1 and #2. Do they belong to N 81? The answer to this question which is crucial for star formation theories (Zinnecker et al. 1993), is not straightforward, because of the complex structure of the SMC with its overlapping layers (McGee & Newton 1981, Stanimirovic et al. 1998).

4.4. Wolf-Rayet candidate

Wolf-Rayet stars as products of massive star evolution are generally very scarce, particularly so in the metal poor SMC galaxy, which contains only nine confirmed stars of this category (Morgan et al. 1991). It is therefore highly desirable to identify and study every single new candidate, such as #7.

A noteworthy feature of our new candidate is its apparent faintness. With $V = 19.64$, it is ~ 3 mag weaker than the faintest W-R stars in that galaxy detected so far from the ground (Azzopardi & Breysacher 1979, Morgan et al. 1991). It is also much fainter than the known Of stars in the SMC (Walborn et al. 1995b). Noteworthy as well is the fact that the small W-R population in the SMC is very peculiar compared to that in our Galaxy. For example, all nine W-R stars are binary systems and all, but one, belong to the nitrogen class. Our candidate may represent the first *single* W-R detected in the SMC. The true nature of this object can only be clarified with STIS spectroscopy during the second phase of our project. Its confirmation would provide new data for improving massive star evolutionary models in the low metallicity domain.

4.5. Future work

We have presented our first results on the SMC "blob" N 81 based uniquely on direct imaging with WFPC2. The high-resolution observations have enabled us to identify the hot star candidates. Forthcoming STIS observations of these stars will provide the stellar spectra. The analysis of the line profiles with non-LTE wind models (Schaerer & de Koter 1997) will allow us to determine the wind properties (terminal velocity, mass loss rate), the effective temperature and luminosity, and to derive constraints on the surface abundances of H, He, and metals (de Koter et al. 1997, Haser et al. 1998). The H-R diagrams so constructed will be compared with appropriate low-metallicity models (Meynet et al. 1994, Meynet & Maeder 1997) to yield the evolutionary status of the stars and to subject the evolutionary scenarios to observational constraints.

Since the SMC is the most metal-poor galaxy observable with very high angular resolution, N 81 provides an important template for studying star formation in the very distant metal-poor galaxies which populate the early Universe. Although other metal-poor galaxies can be observed with *HST* and their stellar content analyzed from color-magnitude diagrams (e.g., I Zw 18: Hunter & Thronson 1995, de Mello et al. 1998), the SMC is the most metal-poor galaxy where spectroscopy of individual stars (required to determine the parameters of massive stars) can be achieved with the highest spatial resolution.

Acknowledgements. We are grateful to Dr. James Lequeux and Dr. Daniel Schaerer who read the manuscript and made insightful comments. We would like also to thank an anonymous referee for suggestions which helped improve the paper. VC would like to acknowledge the financial support from a Marie Curie fellowship (TMR grant ERBFMBICT960967).

References

Azzopardi M., Breysacher J., 1979, A&A 75, 120
Beech M., Mitalas R., 1994, ApJS 95, 517
Bernasconi P.A., Maeder A., 1996, A&A 307, 829

Bodenheimer P., Tenorio-Tagle G., Yorke H.W., 1979, ApJ 233, 85
Bonnell, I.A. Bate M.R., Zinnecker H., 1998, MNRAS 298, 93
Caplan J., Taisheng Y., Deharveng L., Turtle A.J., Kennicutt R.C., 1996, A&A 307, 403
Churchwell E., 1990, A&AR 2, 79
Conti P.S., Garmany D., Massey P., 1986, AJ 92, 48
Davies R.D., Elliott K.H., Meaburn J., 1976, MNRAS 81, 89
de Koter A., Heap S.R., Hubney I., 1997, ApJ 477, 792
de Mello D.F., Schaerer D., Heldmann J., et al., 1998, ApJ 507, 199
Di Benedetto G.P., 1997, ApJ 486, 60
Fruchter A.S., Hook R.N, 1998, PASP, submitted (astro-ph/9808087)
Haser S.M., Pauldrach A.W.A., Lennon D.J., et al., 1998, A&A 330, 285
Henize K.G., 1956, ApJS 2, 315
Herbig G.H., Terndrup D.M., 1986, ApJ 307, 609
Hester J.J., Scowen P.A., Sankrit R., et al., 1996, AJ 111, 2349
Heydari-Malayeri M., Beuzit J.-L., 1994, A&A 287, L17
Heydari-Malayeri M., Testor G., 1982, A&A 111, L11
Heydari-Malayeri M., Testor G., 1983, A&A 118, 116
Heydari-Malayeri M., Testor G., 1985, A&A 144, 98
Heydari-Malayeri M., Testor G., 1986, A&A 162, 180
Heydari-Malayeri M., Le Bertre T., Magain P., 1988a, A&A 195, 230
Heydari-Malayeri M., Magain P., Remy M., 1988b, A&A 201, L41
Heydari-Malayeri M., Van Drom E., Leisy P., 1990, A&A 240, 481
Heydari-Malayeri M. Rosa M., Zinnecker H., Deharveng L., Charmandaris V., 1998, NASA/HST/ESA Press Rlease 98-25, http://oposite.stsci.edu/pubinfo/pr/1998/25
Hill R.J., Madore B.F., Freeman W.L., 1994, ApJ 429, 204
Hillenbrand L.A., 1997, AJ 113, 1733
Holtzman J., Hester J.J, Casertano S., et al., 1995, PASP 107, 156
Hunter D.A., 1995, Rev. Mex. Astron. Astrofis. 3, 1
Hunter D.A., Thronson H.A., 1995, ApJ 452, 238
Israel F.P., Koornneef J., 1988, A&A 190, 21
Israel F.P., Koornneef J., 1991, A&A 248, 404
Israel F.P., Johansson L.E.B., Lequeux J., et al., 1993, A&A 276, 25
Larson R.B., 1992, MNRAS 256, 641
Massey P., Parker J.W., Garmany C., 1989, AJ 98, 1305
McCaughrean M.J., Stauffer J.R., 1994, AJ 108, 1382
McGee R.X., Newton L.M., 1981, Proc. Astron. Soc. Australia 4, 189
Meynet G., Maeder A., Schaller G., Schaerer D., Charbonnel C., 1994, A&AS 103, 97
Meynet G., Maeder A., 1997, A&A 321, 46
Morgan D.H., Vassiliadis E., Dopita M.A., 1991, MNRAS 251, 51P
Palla F., Stahler S.W., 1990, ApJ L47
Prévot M.L., Lequeux J., Maurice E., Prévot L., Rocca-Volmerange B., 1984, A&A 132, 389
Relyea L.J., Kurucz R.L., 1978, ApJS 37, 45
Schaerer D., de Koter A., 1997, A&A 322, 598
Scowen P.A., Hester J.J., Sankrit R., et al., 1998, AJ 116, 163
Shu F.R., Adams F.C., Lizano S., 1987, ARA&A 25, 23
Stanimirovic S., Stavley-Smith L., Dickey J.M., et al., 1998, MNRAS, in press
Tenorio-Tagle G., 1979, A&A 71, 79
Testor, G. Pakull M., 1985, A&A 145, 170
Vacca W.D., Garmany C.D., Shull J.M., 1996, ApJ 460, 914
Walborn N.R., MacKenty J.W., Saha A., White R., 1995a, ApJ 439, L47
Walborn N.R., Haser S.M., Lennon D.J., et al., 1995b, PASP 107, 104
Walborn N.R., Barbá R.H., Brandner W., et al., 1999, AJ 117, 225
Weigelt G., Baier G., 1985, A&A 150, L18
Yorke H.W., Krügel E., 1977, A&A 54, 183
Zinnecker H., McCaughrean M.J., Wilking B.A., 1993, In: Levy E., Lunine J. (eds.) Protostars & Planets III, Univ. Arizona, p. 429